Electron magnetic resonance study of transition-metal magnetic nanoclusters embedded in metal oxides

Vincent Castel and Christian Brosseau*

Laboratoire d'Electronique et Systèmes de Télécommunications, Université de Bretagne Occidentale, CS 93837, 6 Avenue Le Gorgeu, 29238 Brest Cedex 3, France

(Received 25 October 2007; revised manuscript received 28 February 2008; published 10 April 2008)

Here, we report on the results of an electron magnetic resonance (EMR) study of a series of Ni/ZnO and Ni/γ-Fe_2O_3 nanocomposites (NCs) to probe the resonance features of ferromagnetic (FM) Ni nanoclusters embedded in metal oxides. Interest in these NCs stems from the fact that they are promising for implementing the nonreciprocal functionality employed in many microwave devices, e.g., circulators. We observe that the EMR spectrum is strongly affected by the metallic FM content and its environment in the NC sample. We report the existence of broad and asymmetric features in the EMR spectra of these NCs. Our temperature dependent EMR data revealed larger linewidth and effective g factor, in the range of 2.1–3.7 (larger than the free electron value of ≈ 2), for all samples as temperature is decreased from room temperature to 150 K. The line broadening and asymmetry of the EMR features are not intrinsic properties of the metallic nanophase but reflect the local (nonmagnetic or magnetic) environment in which they are embedded. Furthermore, the results of a systematic dependence of the room temperature EMR linewidth and resonant field on the Ni content and the corresponding effective microwave losses measured in previous works show a remarkable correlation. This correlation has been attributed to the dipolar coupling between magnetic nanoparticles in the NCs.

DOI: 10.1103/PhysRevB.77.134424 PACS number(s): 75.50.Tt, 75.75.+a, 76.30.Fc, 76.50.+g

I. INTRODUCTION

Interest in the polarization and magnetization mechanisms in nanocomposites (NCs) is on the rise. From the fundamental point of view, the main scientific drivers are the multiplicity of new and interesting effects, e.g., product property such as magnetoelectricity,[1–4] and the observation that many of the ideas central to the understanding of two-dimensional electromagnetism and magnetism indicate the need for new theoretical and experimental approaches. Respective systems might be realized in granular mixtures, layered compounds, thin films, or artificial multilayers. Another reason to give some attention to magnetic NCs is the current increase in interest in biological physics and in the development of new pharmaceutical products.[5–9] The particular interest among the biophysical and chemical sciences is triggered by the fact that plasmonic NCs can provide promising platforms for the development of multimodal imaging and therapy approaches.[10,11] From the practical side, such studies are important for developing techniques that are able to produce nanostructures in a controlled manner. However, expectations for integrated nanoelectronic devices exhibiting new functionalities will become more realistic when there is complete understanding of the microscopic mechanisms that control changes in electronic structure that scale with the cluster dimensions.

While much attention has focused on exploring the microstructure of materials by using conventional methods of characterization, recent work has recognized the value of conventional electron magnetic resonance (EMR) techniques (see, e.g., Refs. 12–14) which can reveal both the average magnetic behavior and its microscopic inhomogeneity. These techniques have proven to provide reliable approaches to the stability of nanoparticle dispersions which can be affected by aggregation and agglomeration due to their high surface energy, secondary crystallization, and Ostwald ripening, just to name a few indicative ones.[12,15–19] At this length scale, conduction and magnetic properties considerably deviate from bulk, e.g., by showing a significant enhanced magnetic moment for sizes up to a few hundred atoms.[4,9] Within this context, a powerful attribute of the EMR is its ability to experimentally probe local scale.

As yet, few experimental approaches for the EMR analysis of magnetic NCs have been discussed. Only a few selected magnetic nanoparticle systems, including γ-Fe_2O_3 (Refs. 12, 15, and 16) and ferrites,[20–23] were investigated by the EMR methods. So far, hardly any data exist on the EMR characterization of magnetic metal and/or metal oxide NCs. It is also worth emphasizing that several analytical[24] and numerical[25,26] approaches have been put forward to analyze the resonance spectra of magnetic submicron particles. Despite this motivation to develop a full understanding of ferromagnetic (FM) metallic nanoclusters dispersed into a variety of (magnetic or not) hosts from EMR, several basic features in the gigahertz EMR modes remain unclear. In particular, there is no simple theory which allows the measured spectrum to be related to the underlying microstructure. Another basic issue is to determine whether the linewidth is an intrinsic feature of metallic clusters or arises as a consequence of surface interactions or other perturbations.

Our original intent for the present work was to investigate Ni/ZnO and Ni/γ-Fe_2O_3 NCs. A series of recent microwave frequency-domain spectroscopy (gigahertz) studies of the quasistatic effective permittivity and magnetic permeability posed fundamental questions concerning polarization and magnetization mechanisms in these NCs.[27–32] Here, these materials were chosen because our group has previously published detailed accounts of experimental and modeling approaches on the static magnetic and microwave response of the samples under study.[33–38] This analysis allowed us to

TABLE I. Selected physical properties of the powders investigated in this study.

Powder	ZnO	γ-Fe_2O_3	Ni
Average particle size[a–d]	49 nm	23 nm	35 nm
Powder color	White	Brown	Black
Specific surface area BET[a] ($m^2\ g^{-1}$)	22	51	15.6
Morphology[c]	Elongated	Nearly spherical, faceted	Spherical
Crystal phase[a,d]	Wurtzite	Maghemite (Cubic spinel)	*Fm*3*m* (225) ccp
Density[a] ($g\ cm^{-3}$)	5.6	5.2	8.9

[a]From manufacturer product literature.
[b]Determined from specific surface area.
[c]Checked by TEM images.
[d]Determined by XRD. In the XRD analysis, the possible influence of strain on the online broadening was neglected. This may result in an underestimate of the particle size.

simulate magnetization dynamics on solving the Landau–Lifshitz–Gilbert equation coupled to the Bruggeman effective medium approach. Traditionally, particle and aggregate size information are considered irrelevant to the wave transport since rapid oscillations of the electromagnetic wave on length scales larger than any scale ξ of the medium inhomogeneities are integrated out in the conventional effective medium analysis, where it is specifically assumed that $\xi \ll \lambda$ with λ the wavelength of the probing wave, and thereby the NC can be treated as a structureless continuum medium.[30,31,34–36,39,40] Some very recent work has demonstrated that ferromagnetic resonance (FMR) measurements of these NCs,[37,38] or of hot isostatic pressed (hipped) polycrystalline yttrium iron garnet[41] are very sensitive to details of the spatial magnetic inhomogeneities. Although these studies have advanced the understanding of wave transport phenomena in granular NCs, striking discrepancies remain between experiments and corresponding results obtained from existing phenomenological models and numerical simulations. An important question of broad fundamental interest is why the effective permittivity and magnetic permeability appear to be very sensitive to the details of the nanoparticle cluster structure, thus suggesting a breakdown of the continuum-level modeling and bringing NC physics concepts to light. The answer to this question constitutes the key for understanding the response of magnetic clusters to electromagnetic probes.

In the present study, we report on a detailed EMR study of magnetic metal and/or metal oxide NCs. This paper provides two main results. By varying the Ni volume fraction in the samples, we observed that the EMR signal reflects the properties of the metallic FM nanophases as well as the local nonmagnetic or magnetic environment in which they are embedded. Our data also indicated an empirical correlation between the systematic dependence of EMR linewidth and

TABLE II. Overview of NCs compositions: f_x denotes the volume fraction of the X species, f_p is the porosity of the samples and f_{resin} is the volume fraction of resin. The uncertainty on f_x is typically of the order of 5%.

Material designation	f_{Ni}	f_{ZnO}	f_p	f_{resin}	f γ-Fe_2O_3
nNiZ1	0.49	0.08	0.28	0.15	
nNiZ2	0.42	0.17	0.27	0.14	
nNiZ3	0.38	0.21	0.26	0.15	
nNiZ4	0.33	0.26	0.25	0.15	
nNiZ5	0.29	0.30	0.26	0.15	
nNiZ6	0.25	0.35	0.25	0.15	
nNiZ7	0.18	0.44	0.23	0.14	
nNiZ8	0.09	0.54	0.22	0.15	
nNiZ9	0	0.63	0.21	0.16	
1–nNiF	0.08		0.26	0.13	0.53
2–nNiF	0.17		0.25	0.14	0.44
3–nNiF	0.29		0.27	0.12	0.32
4–nNiF	0.50		0.26	0.15	0.09
5–nNiF	0.04		0.26	0.25	0.55

resonant field on the Ni content and the corresponding microwave loss features.

The rest of the paper is organized as follows. Section II gives some background on the samples we have investigated and discusses technical details on the EMR characterization. This is followed in Sec. III by a presentation of an experimental analysis of the effects of varying the Ni content in the NCs on the EMR spectra. A comparison with previous FMR linewidth data and effective microwave losses is given in Sec. IV. Next, Sec. V presents the main conclusions of this study and we make some comments regarding possible implications of these results.

II. EXPERIMENT

The same samples were used as in a previous study.[33] Room temperature-pressed NC compacts were made under the application of a uniaxial pressure of 64 MPa for 2 min. The morphology and size of the starting powders (Table I) were determined by transmission electron microscopy (TEM) by using a 200 kV Phillips apparatus. Bright field TEM images indicate that γ-Fe_2O_3 and Ni particles are homogeneous with nearly spherical shape, whereas the wurtzite-type ZnO particles are rod shaped with an aspect ratio of about 3:1. The phase purity was checked by x-ray powder diffraction (XRD) by using Cu $K\alpha_1$ radiation, and the crystallite sizes were determined from the full width at half maximum of the strongest reflection by using the Williamson-Hall method after applying the standard correction for instrumental broadening. The average crystalline sizes of the samples were also determined from analysis of bright field that cross-sectional TEM images were found to be consistent with the ones obtained from XRD measurements.[30–34] The XRD analysis of spherelike clusters suggests that Ni existed in the form of metal. These clusters, composed of Ni nanoparticles, are randomly and uniformly distributed in the matrix and are isolated from each other by the metal oxide and epoxy phases. The Ni cluster size increases with the Ni content. The metallic nanoparticle tends to be oxidized, arising from the large surface-area-to-volume ratio and the high electronegativity of metallic nickel. Although not studied in detail, the presence of secondary phases, e.g., NiO, was estimated to be less than 0.3 vol % from XRD. In addition, Ni nanoparticles can be protected from oxidation by encapsulation in the epoxy phase.

The EMR experiments were performed in two sets of samples (see Table II). The first series (Ni/ZnO) comprising nominal Ni volume fractions in the range of 0%–49% consisted of mixtures of Ni and ZnO nanoparticles and epoxy resin (15 vol %). The second series (Ni/γ-Fe_2O_3) had nominal Ni volume fractions in the range of 4%–50% and γ-Fe_2O fractions were chosen to maintain the total content of the magnetic phase constant $\approx$60 vol %. For the two sets of NCs, the residual porosities were estimated to be between 21 and 28 vol %.

For the present EMR measurements, samples were cut to pieces of about $1\times1\times1$ mm^3. EMR signals were recorded on a heterodyne spectrometer in a continuous wave mode X-mode microwave (F=9.4 GHz) with a 500 mW Varian klystron, a Bruker resonance TE_{102} cavity, a Varian electromagnet with maximum field amplitudes of 800 mT, and a nitrogen flux cryosystem (Oxford Instruments) for low-temperature measurements in the range from 150 K to room temperature (RT). For g-factor calibration, the 1,1-diphenyl-2-picrylhydrazyl standard has been used (g=2.0037). The EMR signals recorded were the first derivatives of the power absorption, dP/dH, as a function of the applied magnetic field H by using 100 kHz modulation amplitude and lock-in technique (EG&G Princeton) for calculations of g factors, peak-to-peak linewidths (ΔH_{pp}), and resonance field (H_{res}). For the g-factor measurements, the cavity frequency ν was measured at each temperature and H_{res} is determined by the location of the zero of the absorption derivative. Then, $g=0.714\,48\times10^{-6}\nu/H_{res}$, where ν is in gigahertz and H_{res} in kilo-oersted. The EMR measurement was performed on cooling the sample.

EMR signals were also obtained for neat nanoparticles by using either powders placed in an EMR tube, and pumped to $<10^{-3}$ Pa in order to eliminate the moisture and oxygen effect, or in loose packed form with 15 vol % epoxy. For both samples, the EMR line cannot be accurately fitted to a single Lorentzian line shape (not shown). Figures 1 and 2 show that H_{res} (ΔH_{pp}), for both neat and compacted powders of Ni and γ-Fe_2O_3, appreciably increases (decreases) with T for T_s in the range of 150–300 K. The broadening of the EMR feature is sharply decreased by upshifting the resonance field. Systematic EMR characteristics follow the same monotonic trends; however, the data reveal that the dilution of nanoparticle powder in the epoxy host matrix and compaction have for effect to downshift the EMR line and to decrease its peak width compared to the neat powder EMR features. The EMR linewidth is affected by inhomogeneities and is quite large, i.e., 0.85–2.6 kOe. The difference between powder and loose packed form with epoxy can be attributed to some aspects of the microstructure, such as porosity, grain boundaries and other extended defects, the presence of local strains, or anisotropy in the randomly oriented magnetic clusters. Figure 3 illustrates that g rapidly decreases with increasing T for the neat Ni powder, whereas for γ-Fe_2O_3 powder, g shows little T dependence and does not significantly deviate from $g\approx2.1-2.2$. A similar behavior has been reported in ferrite nanoparticles.[12] For ease of comparison, data are plotted as $g(T)/g(\mathrm{RT})$. Part of the g shift with lowering T can be attributed to the increase in the demagnetizing field. We would like also to emphasize that no measurable EMR signal for ZnO nanoparticle powder was detected.

For our low conductivity NCs and considering the measured values of the effective electromagnetic parameters of these NCs,[31,37,38] we find that the skin depth is in the 10^2-10^3 mm size range in the gigahertz frequency range, i.e., much larger than the sample thickness. Thus, one can safely assume a full and homogeneous penetration of the microwaves into our samples. In composites with uniform dispersions of magnetic nanoparticles, the conductivity of the NC is mainly determined by the interparticle distance and eddy currents, produced within the particle is extremely small at high frequency, which are limited to individual particles or aggregates. We note that Ramprasad *et al.*[27] have shown, in their phenomenological modeling of the properties

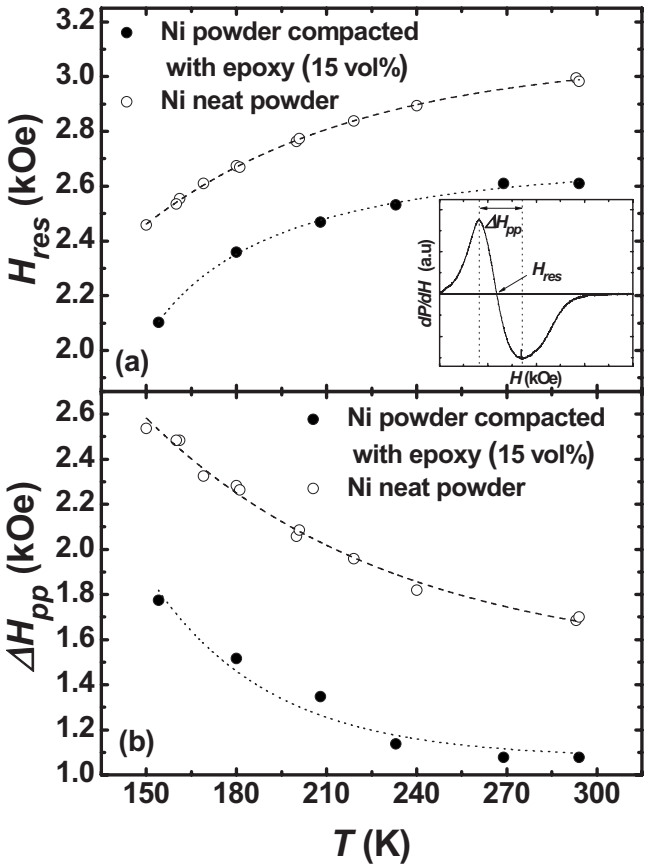

FIG. 1. (a) The line position, H_{res}, as a function of temperature for neat Ni powder and a Ni (56 vol %) powder compact with 15 vol % epoxy (see text for details). The inset shows that the resonant field H_{res} is determined by the location of the zero of the absorption derivative. The dotted and dashed lines serve as guides for the eye. (b) Same as in (a) for the peak-to-peak linewidth ΔH_{pp} corresponding to the peak-to-peak separation in the absorption derivative [inset of (a)].

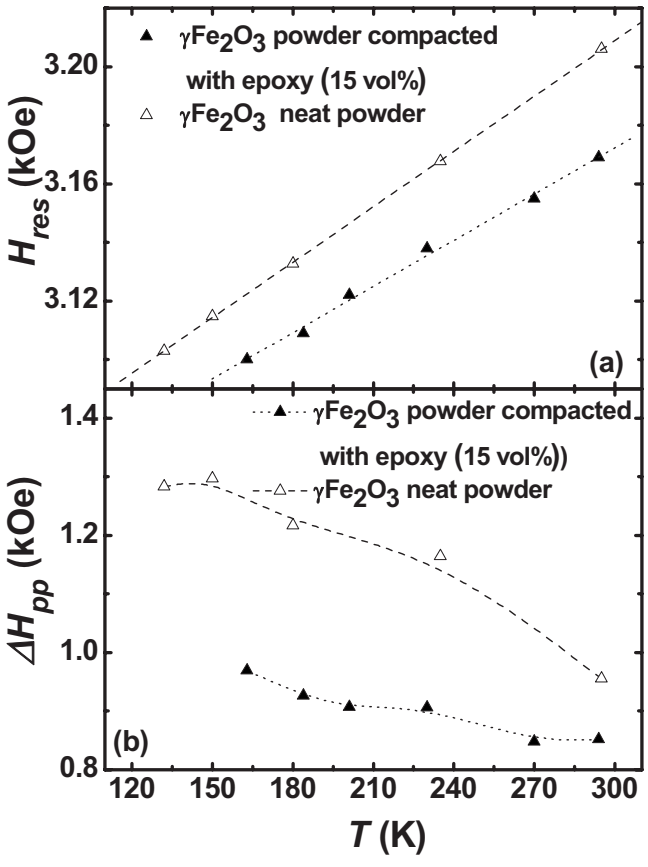

FIG. 2. (a) The line position, H_{res}, as a function of temperature for neat γ-Fe_2O_3 powder and a γ-Fe_2O_3 (56 vol %) compact with 15 vol % epoxy. The dotted and dashed lines serve as guides for the eyes. (b) Same as in (a) for the peak-to-peak linewidth ΔH_{pp}.

of magnetic nanoparticle composites, that in the 0.1–10 GHz frequency range, particles with radii smaller than 100 nm are expected to encounter negligible eddy current losses. This was found true even at high particle volume fraction, when clustering of particles could result in aggregates much larger than the actual particles. Furthermore, no signature for percolation threshold is apparent for the data collected; thus, we infer from the Ni content dependence of σ_{dc} that the Ni nanoaggregates should be separated in the ZnO matrix. It has been recognized by now that in ferromagnetic NCs, the shielding and dissipation due to eddy currents rapidly diminish with decreasing the particle size. This has for effect to reduce the dielectric losses in metallic nanoparticles.

III. ELECTRON MAGNETIC RESONANCE LINEWIDTH PARAMETERS

We now present the data underlying our conclusions summarized above. Full sets of absorption versus field derivative profiles, shown in arbitrary units, which correspond to representative EMR spectra of Ni/ZnO and Ni/γ-Fe_2O_3 NCs, were obtained in the restricted temperature range from 300 to 150 K. Typical spectra are displayed in Figs. 4(a) and 4(b) at six different temperatures for Ni/ZnO (Ni content of 17.5 vol %) and Ni/γ-Fe_2O_3 (Ni content of 50.3 vol %) NCs, respectively. Note first that the EMR spectra display a severely distorted line shape suggestive of inhomogeneous broadening, which is typical of superparamagnetic resonance spectra.[25] Unfortunately, the spectra cannot be meaningfully deconvoluted. Possible explanations range from size and shape distributions to magnetic anisotropy (see, for example, Refs. 25 and 26). A consensus on the cause of these has yet to be established partly because it is difficult to make quantitative evaluations of the EMR line in composites of fine magnetic particles and also because there may not be a single cause.

To analyze the temperature dependence of the EMR spectra, ΔH_{pp} and H_{res} are shown in Fig. 5 (Fig. 6) as a function of temperature for the Ni/ZnO NCs (Ni/γ-Fe_2O_3 NCs). The inset of Fig. 1 indicates how ΔH_{pp} and H_{res} were actually measured. The data of the lower panels of Figs. 5 and 6 serve to make four important points. First, although different in detail, the T dependence of ΔH_{pp} in Figs. 5 and 6 has important features in common, namely, as T is increased, ΔH_{pp} monotonically decreases. Also, the line shape becomes quite asymmetrical at the lower temperatures. For the three lowest Ni volume fractions in Ni/γ-Fe_2O_3 NCs, a very weak de-

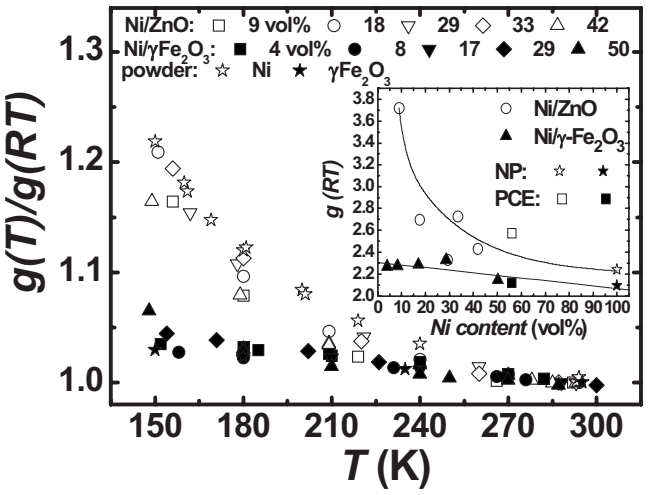

FIG. 3. Effective g factor, normalized to the RT value g(RT), of Ni/ZnO (open symbols), and Ni/ γ-Fe_2O_3 (filled symbols) NC samples as a function of temperature. The corresponding values for the neat powders of Ni (open stars) and γ-Fe_2O_3 (filled stars) have been shown for comparison. The inset shows g(RT) versus the Ni content in the Ni/ZnO (open circles) and Ni/ γ-Fe_2O_3 (filled triangles) NC samples, Ni powder compact (open square) with 15 vol % epoxy and γ-Fe_2O_3 powder compact (filled square) with 15 vol % epoxy [phosphorus-containing (PCE)], and neat Ni (open star) and γ-Fe_2O_3 (filled star) powder (NP) samples. The solid lines serve as guides for the eyes.

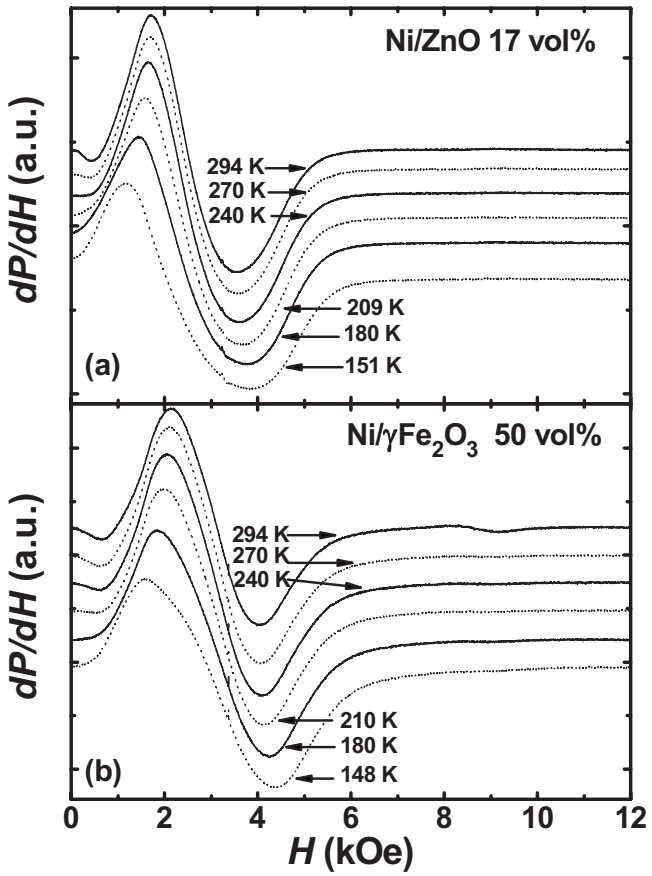

FIG. 4. (a) X-band EMR spectra (absorption derivative) for a representative Ni/ZnO NC sample (Ni content of 17.5 vol %) and different temperature values. (b) X-band EMR spectra (absorption derivative) for a representative Ni/ γ-Fe_2O_3 sample (Ni content of 50.3 vol %) and different temperature values.

cline around 1.1 kOe is observed. At low temperatures, the spin-spin interactions cause spin dynamics to freeze out, and spins essentially behave as static spins. At higher temperatures, when the time scale of the dynamics of the spins is fast, it might be expected that the conduction electron spin-lattice relaxation time in metals, T_1, is the characteristic time for the return to thermal equilibrium of a spin system driven out of equilibrium by the microwave field at resonance. It is well established that in pure metals, T_1 is limited by the scattering of conduction electrons by the random spin-orbit potential of nonmagnetic impurities or phonons.[14] These changes in $\Delta H_{pp}(T)$ and $g(T)$ are reflected in the motional narrowing of the EMR line.[15,25] Second, when these values are compared to the experimental data of neat and compacted powder with epoxy, i.e., Figs. 1 and 2, it is seen that the dependence of ΔH_{pp} on T matches rather well that for neat powder, except for the Ni/ γ-Fe_2O_3 NCs containing the two largest Ni volume fractions. We also notice that for the Ni/ γ-Fe_2O_3 sample with 50 vol % Ni, one recovers very similar values of ΔH_{pp} than for those displayed in Fig. 5 for Ni/ZnO samples. Thus, the line broadening is not an intrinsic feature of Ni but arises as a consequence of surface interactions, reflecting the fact that interaggregate interactions induce collective behavior between the magnetic nanophases. It seems likely that the interfaces play a key role in determining the ultimate performance of magnetic nanostructures: the surface anisotropy and magnetization significantly modify the static states and dynamic properties.[42] Further, the broadening of the EMR features is sharply increased for a large Ni content in Ni/ γ-Fe_2O_3 NCs. That the H_{res} versus T dependences do not map the H_{res} of powdered samples is also a noticeable fact. A natural question is why we observe a substantial downshift of the EMR line of the magnetically diluted samples in comparison with neat powders. It is rather likely that this downshift is a manifestation of powder compaction during sample fabrication. Indeed, we observed (not shown) an apparent correlation between the residual porosity and the effective density of the NC samples, e.g., we simultaneously measured a 30% drop of the porosity with a 10% increase in the density as the applied pressure during the compact fabrication process is changed from 33 to 230 MPa. Third, it is worth noting that ΔH_{pp} for Ni/ZnO NCs is larger than the corresponding value of ΔH_{pp} for Ni/ γ-Fe_2O_3 NCs for a given Ni concentration. Interestingly, there is also a clear trend toward lower H_{res} for smaller temperature, as displayed in Fig. 5. Fourth, the EMR lines continuously shift to high fields as the temperature is increased. For the Ni/ZnO NCs, the temperature variation $H_{res}(T)$ resembles [see Fig. 5(a)] that observed for neat or compacted powder, in stark contrast to what is observed for Ni/ γ-Fe_2O_3 NCs, i.e., Fig. 6(a).

Figure 3 summarizes the dependence of the lowering of the effective g factor on temperature for the two kinds of NCs. The inset shows the actual values of g(RT). For Ni/ZnO NCs, these values rapidly fall to the g factor corre-

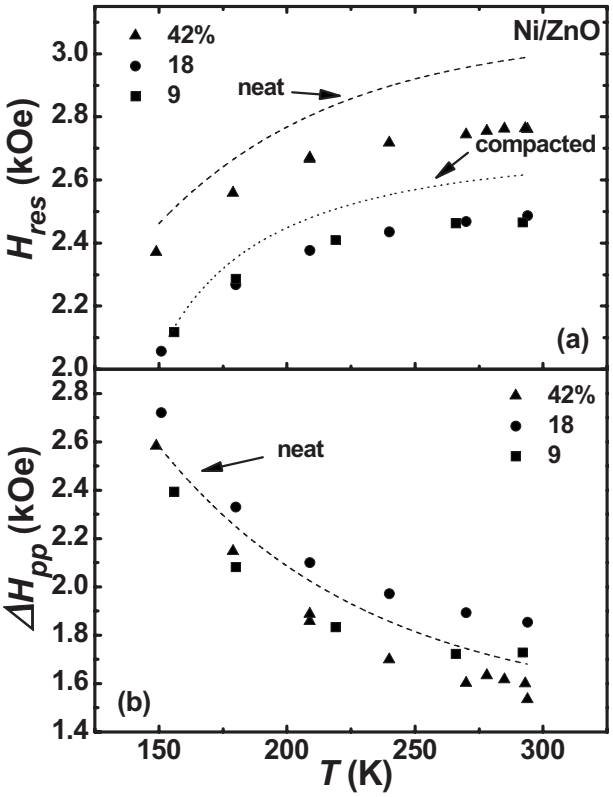

FIG. 5. (a) The line position, H_{res}, as a function of temperature for Ni/ZnO NC samples. The number indicates the Ni volume fraction. For the purpose of comparison, we have represented the values of H_{res} for neat Ni powder and a Ni (56 vol %) powder compact with 15 vol % epoxy as dashed and dotted lines, respectively. (b) Same as in (a) for the peak-to-peak linewidth ΔH_{pp}. For the purpose of comparison, we have represented the values of H_{res} for neat Ni powder and a Ni (56 vol %) powder compact with 15 vol % epoxy as dashed and dotted lines, respectively.

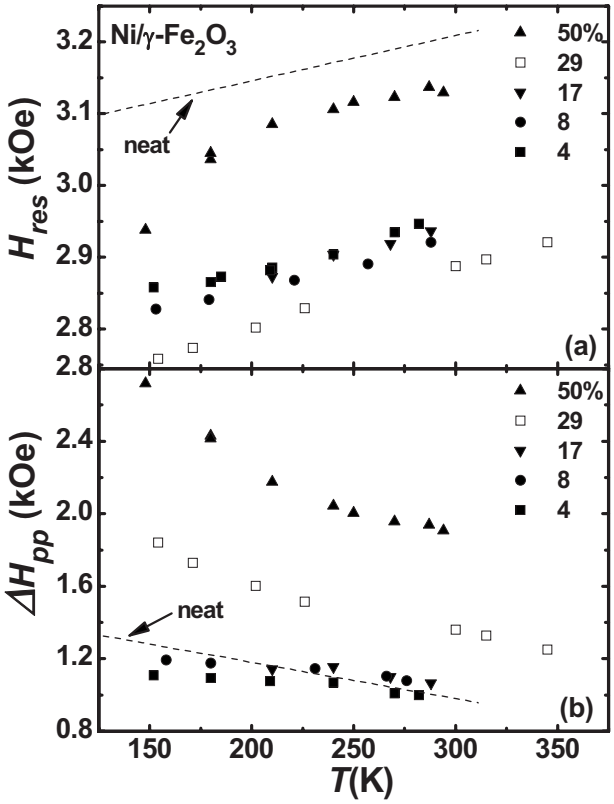

FIG. 6. Same as in Fig. 5 for Ni/ γ-Fe_2O_3 samples. For the purpose of comparison, we have represented the values of H_{res} for neat Ni powder and a Ni (56 vol %) powder compact with 15 vol % epoxy as dashed and dotted lines, respectively.

sponding to neat powder $[g(RT) \approx 2.2]$. By contrast, g(RT) is practically constant for Ni/ γ-Fe_2O_3 NCs. The clear and systematic decrease in the g factor can be found up to the highest accessible temperature of 300 K. The experimental behavior could arise from several sources. First, there is motional narrowing. Another possible mechanism is the interplay of demagnetizing field effects and of the presence of short-range magnetic ferrimagnetic ordering due to the γ-Fe_2O_3 nanoparticles.

Figure 7 (Fig. 8) illustrates how ΔH_{pp} and H_{res} at RT change as a function of the metallic FM nanophase content for the Ni/ZnO NCs (Ni/ γ-Fe_2O_3 NCs). For Ni/ZnO NCs, ΔH_{pp} significantly increases as Ni volume fraction is increased followed by a sharp drop at Ni content of $\approx$30 vol %, while in the same Ni fraction range, ΔH_{pp} monotonically increases for the Ni/ γ-Fe_2O_3 specimens. These data serve to make two further points. First, the broadening of the EMR line for Ni/ γ-Fe_2O_3 samples is sharply increased by increasing the Ni volume fraction. We interpret the broadening of the EMR features in these samples as arising from the strong collective magnetostatic intergranular interactions of the nanosized FM clusters with the surrounding ferrimagnetic matrix. Second, it is interesting to relate the maximum of ΔH_{pp} to the electrical transport properties of the Ni/ZnO NCs characterized by the four-point probe technique.[37] In Ref. 37, we discussed a set of electrical transport data of these materials and observed that the RT dc conductivity σ_{dc} versus Ni content data for Ni/ZnO NCs collected at low field exhibit an S-shaped curve (not *percolativelike* process) with an exponential increase between 10 and 30 vol % Ni and a change of slope at about 30 vol % Ni.

Generally, in the solid state, we classify EMR lines into those that are homogenously broadened and those that are inhomogeneously broadened.[13,14] The main contributions to homogeneous broadening are the magnetic dipolar coupling, spin-lattice interaction, interaction with radiation field, and motionally narrowing fluctuations of local fields.[13,14] For the inhomogeneous case, the line broadening mechanism distributes the resonance frequencies over an unresolved band, e.g., inhomogeneous external magnetic field, anisotropic interactions in the randomly oriented set of spins, unresolved hyperfine structure, and strain distribution. Thus, the distribution in local fields will make the spins in various parts of the sample feel different field strengths. Here, in the analysis of our FMR spectra of the NCs under study here,[37] we found that inhomogeneity based line broadening mechanisms, due to the damping of surface and/or interface effects and interparticle interaction, affect the FMR effective linewidth. These remarks suggest that the ΔH_{pp} versus T and Ni content is most likely associated with two contributions to the observed EMR linewidth: on the one hand, there is the homo-

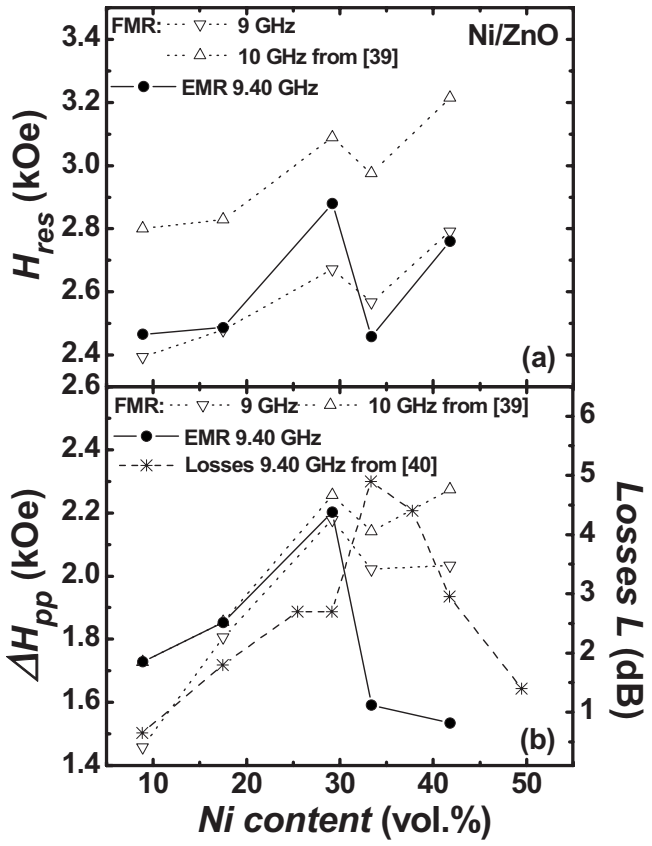

FIG. 7. EMR line peak-to-peak width $\Delta H_{\mathrm{p.p.}}$ and position, H_{res}, (9.40 GHz) plotted as a function of the Ni content in the Ni/ZnO NC samples at RT. Comparison with FMR data (9 and 10 GHz) from Ref. 39 and microwave loss data (9.40 GHz) from Ref. 40.

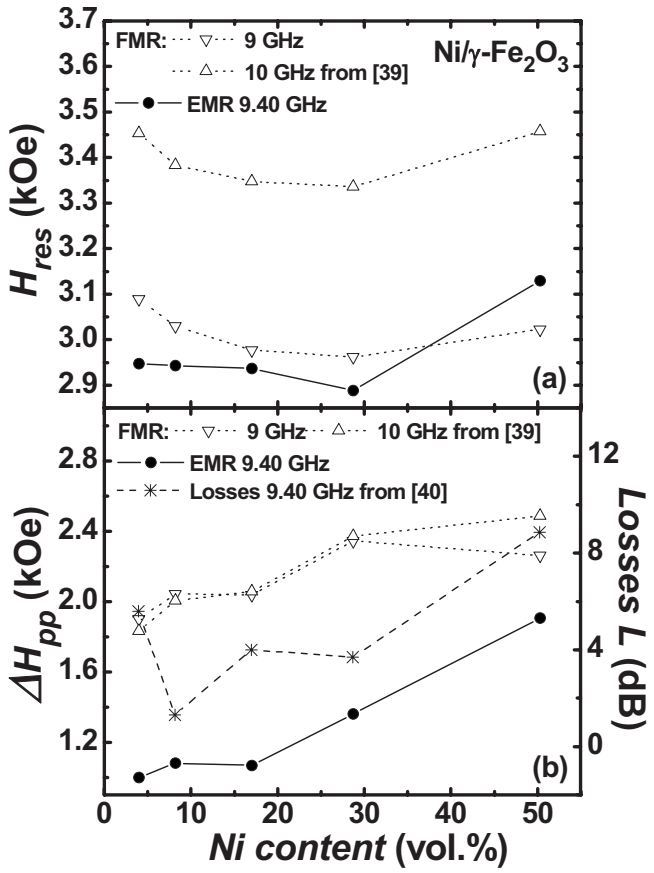

FIG. 8. Same as in Fig. 7 for Ni/ γ-Fe_2O_3 samples.

geneous line broadening mechanism involving dipolar interaction and spin-lattice relaxation, which is strongly temperature dependent (motional narrowing). On the other hand, the unsymmetrical line shape, especially at low temperatures, is an indication that the EMR is broadened in an inhomogeneous manner and the EMR linewidth is expected to increase as a function of magnetic field.[37]

IV. COMPARISON WITH FERROMAGNETIC RESONANCE SPECTRA AND MICROWAVE LOSSES

It may be meaningful to compare our EMR parameters to values of the linewidths measured over the 9–10 GHz frequency range recently reported in FMR experiments, investigating the surface anisotropy contribution to the anisotropy of Ni and γ-Fe_2O_3 nanoparticles,[37] and to effective microwave losses measured in order to probe the evolution of large-wave-vector spin wave modes in these NCs.[38] The FMR response of magnetic nanostructures is a rich area in its own right, and several models,[43,44] e.g., two-magnon scattering theory, have been applied to the problem of magnetic heterogeneities in coarse-grained heterostructures. From these FMR measurements,[37] it was pointed out that the characteristic intrinsic damping dependent on the selected material and the damping due to surface and/or interface effects and interparticle interaction were estimated. Inhomogeneous damping due to surface and/or interface effects increases with diminishing particle size, whereas damping due to interactions increases with increasing volume fraction of magnetic particles (i.e., reducing the separation between neighboring magnetic phases) in the composite.

Figures 7 and 8 summarize the main findings of this work. The upper and lower panels in Figs. 7 and 8 provide a direct comparison of ΔH_{pp} and H_{res} as a function of Ni content and at RT between, on the one hand, the EMR (9.40 GHz) features and the nominal (9 and 10 GHz) uniform FMR mode, and on the other hand, the nominal (9.40 GHz) microwave losses. A number of interesting features are worth remarking. First, all of the curves show nonmonotonic variations. Second, as can be realized from these graphs, the striking main feature is the qualitative similarity in the three types of measurements. Third, as seen in Figs. 7 and 8, substituting a nonmagnetic by a magnetic host matrix not only shifts the position of the resonance but also sensitively affects its linewidth. This is caused by locally changing the interactions between magnetic nanoparticles. It has been recognized that a shortening of T_1 can result from weak dipole interactions, whereas strong interactions may result in slowing down of the relaxation.[45] The analysis of the FMR spectra was interpreted in Ref. 37 as arising from aggregates of magnetic nanoparticles, each of which resonates in an effective magnetic field composed of the applied field, the average (magnetostatic) dipolar field, and the randomly oriented magnetic anisotropy field. The importance of the Ni concentration has

also been discussed in relation to measurements of the spin wave group velocity induced by the samples.[38] The presence of nonmagnetic phases of specific type and volume fraction offers the possibility of controlling the magnetic and microwave properties of NCs.

V. CONCLUDING REMARKS

In summary, a systematic EMR study in Ni/ZnO and Ni/ γ-Fe_2O_3 NCs, for temperatures ranging from 150 up to RT, has been presented. Two compounds with different properties (diamagnetic ZnO and ferrimagnetic γ-Fe_2O_3) and structural disorder were chosen in order to vary the magnetic interactions between the nanoparticles in these heterostructures. There are general reasons to expect that the EMR line broadening and position are not intrinsic features of the metallic FM content, but arise as a consequence of the interaction between aggregates and other interface perturbations. The motional narrowing offers an explanation for the wide variation in the degree of broadening of the EMR line as a function of temperature. The strength of the coupling, as manifested by the EMR linewidth, can be significantly modified by the metallic FM content. One very interesting finding is that there is a clear correlation between EMR linewidth, the corresponding FMR features, and the effective microwave losses measured in these heterostructures. The correlation found here is far from trivial and we regard it as motivation for the development of models underlying the process of resonance in granular heterostructures in which all the details take place. More specifically, although a large number of theoretical calculations have been performed to understand the phenomenon of resonance in nanostructures, no first-principles theoretical calculation has been reported to understand the role of the nonmagnetic phase in tuning the FM of nanoclusters which can be a useful reference for experimentalists.

This study is part of a larger effort to identify essential factors governing magnetoelectricity in dense nanostructured compacts and to explore control possibilities due to their rich behaviors under magnetic and electric perturbations.[46] There are (at least) three directions in which the present work could be extended. First, one wishes to know if our experimental findings do extend to functional multiferroic NCs motivated by the desire to be able to simultaneously manipulate different combinations of microwave properties by the application of external fields. Second, the question begs to be asked: what is the impact of having extremely dense nanocompacts, e.g., by using hot isostatic pressing in order to have a nearly complete elimination of porosity, on EMR linewidths. Third, numerous experimental challenges exist when considering magnetic NCs because they offer a promising avenue toward nanoelectronics and spintronics. EMR can give important insights complementing information from direct studies of the morphological structure of magnetic nanoclusters. Investigations at these length scales are in their infancy, and much room exists for improvement. There remains significant work ahead in continuing to understand the growth modes of nanoparticle aggregates, e.g., for Ni clusters containing up to 800 atoms, regularly spaced peaks in the mass spectra of a certain magic cluster sizes have been interpreted as icosahedral growth patterns.[47] The applicability of metals in nanoelectronic and spintronic devices in which information is processed by using electron spins will depend on a sufficiently long spin lifetime, i.e., long T_1 or narrow EMR linewidth.[48] We hope to discuss the magnetism of Ni clusters and the resulting microwave frequency-domain spectroscopy in future work.

ACKNOWLEDGMENTS

One of the authors (V.C.) gratefully acknowledges financial support from the Conseil Régional de Bretagne. We wish to thank J. Ben Youssef for helpful conversations. We also wish to thank N. Kervarec for her assistance in EMR experiments.

*Also at Département de Physique, Université de Bretagne Occidentale. brosseau@univ-brest.fr

[1] J. Baker-Jarvis and P. Kabos, Phys. Rev. E **64**, 056127 (2001).
[2] J. Zhai, J. Li, D. Viehland, and M. I. Bichurin, J. Appl. Phys. **101**, 014102 (2007).
[3] R. S. Devan and B. K. Chougule, J. Appl. Phys. **101**, 014109 (2007).
[4] G. B. Smith, in *Introduction to Complex Mediums for Optics and Electromagnetics*, edited by W. S. Wieglhofer and A. Lakhtakia (SPIE, Bellingham, 2003).
[5] D. J. W. Grant and H. G. Brittain, *Physical Characterization of Pharmaceutical Solids* (Dekker, New York, 1995).
[6] B. E. Rabinow, Nat. Rev. Drug Discovery **3**, 785 (2004).
[7] S. Y. An, I.-B. Shim, and C. S. Kim, J. Appl. Phys. **97**, 10Q909 (2005).
[8] N. K. Prasad, D. Panda, S. Singh, M. D. Mukadam, S. M. Yusuf, and D. Bahadur, J. Appl. Phys. **97**, 10Q903 (2005).
[9] *Encyclopedia of Nanoscience and Nanotechnology*, edited by H. S. Nalwa (American Scientific, New York, 2004).
[10] A. P. Alivisatos, Nat. Biotechnol. **22**, 47 (2004).
[11] T. A. Larson, J. Bankson, J. Aaron, and K. Sokolov, Nanotechnology **18**, 325101 (2007).
[12] Y. A. Koksharov, D. A. Pankratov, S. P. Gubin, I. D. Kosobudsky, M. Beltran, Y. Khodorkovsky, and A. M. Tishin, J. Appl. Phys. **89**, 2293 (2001); See also M. M. Ibrahim, G. Edwards, M. S. Seehra, B. Ganguly, and G. P. Huffman, *ibid.* **75**, 5873 (2007); P. Dutta, A. Manivannan, M. S. Seehra, N. Shah, and G. P. Huffman, Phys. Rev. B **70**, 174428 (2004).
[13] A. Abragam and B. Bleaney, *Electron Paramagnetic Resonance of Transition Ions* (Clarendon, Oxford, 1970).
[14] C. P. Poole, Jr., *Electron Spin Resonance: A Comprehensive Treatise on Experimental Technique* (Wiley, New York, 1967); See also J. A. Weil, J. R. Bolton, and J. E. Wertz, *Electron Paramagnetic Resonance* (Wiley, New York, 1994).

[15] F. Gazeau, J. C. Bacri, F. Gendron, R. Perzynski, Y. L. Raikher, V. L. Stepanov, and E. Dubois, J. Magn. Magn. Mater. **186**, 175 (1988); F. Gazeau, V. Shilov, J. C. Bacri, E. Dubois, F. Gendron, R. Perzynski, Y. L. Raikher, and V. L. Stepanov, *ibid.* **202**, 535 (1999).
[16] U. Netzelmann, J. Appl. Phys. **68**, 1800 (1990).
[17] R. Kubo, A. Kawabata, and S. Kobayashi, Annu. Rev. Mater. Sci. **14**, 49 (1984).
[18] J. A. A. Perenboom, P. Wyder, and F. Meier, Phys. Rep. **78**, 173 (1981).
[19] W. P. Halperin, Rev. Mod. Phys. **58**, 533 (1986).
[20] V. K. Sharma and F. Waldner, J. Appl. Phys. **48**, 4298 (1977).
[21] I. Hrianca, I. Malaescu, F. Claici, and C. N. Marin, J. Magn. Magn. Mater. **201**, 126 (1999).
[22] K. Nagata and I. Ishishara, J. Magn. Magn. Mater. **104-107**, 1571 (1992).
[23] R. Massart, D. Zins, F. Gendron, M. Rivoire, R. V. Mehta, R. V. Upadhyay, P. S. Goyal, and V. K. Aswal, J. Magn. Magn. Mater. **201**, 73 (1999).
[24] R. S. de Biasi and T. C. Devezas, J. Appl. Phys. **49**, 2466 (1977).
[25] Y. L. Raikher and V. I. Stepanov, Phys. Rev. B **50**, 6250 (1994).
[26] J. Kliava and R. Berger, J. Magn. Magn. Mater. **205**, 328 (1999).
[27] R. Ramprasad, P. Zurcher, M. Petras, M. Miller, and P. Renaud, J. Appl. Phys. **96**, 519 (2004).
[28] L. Spinu, J. O'Connor, and H. Srikanth, IEEE Trans. Magn. **37**, 2188 (2001).
[29] J. P. Calame, A. Birman, Y. Carmel, D. Gershon, B. Levush, A. A. Sorokin, V. E. Semenov, D. Dadon, L. P. Martin, and M. Rosen, J. Appl. Phys. **80**, 3992 (1996).
[30] C. Brosseau and P. Talbot, IEEE Trans. Dielectr. Electr. Insul. **11**, 819 (2004).
[31] C. Brosseau and P. Talbot, J. Appl. Phys. **97**, 104325 (2005).
[32] J. B. Youssef and C. Brosseau, Phys. Rev. B **74**, 214413 (2006).
[33] C. Brosseau, J. Ben Youssef, P. Talbot, and A.-M. Konn, J. Appl. Phys. **93**, 9243 (2003).
[34] S. Mallegol, C. Brosseau, P. Queffelec, and A.-M. Konn, Phys. Rev. B **68**, 174422 (2003).
[35] C. Brosseau, S. Mallegol, P. Queffelec, and J. Ben Youssef, Phys. Rev. B **70**, 092401 (2004).
[36] C. Brosseau, S. Mallegol, P. Queffelec, and J. Ben Youssef, J. Appl. Phys. **101**, 034301 (2007).
[37] V. Castel, J. Ben Youssef, and C. Brosseau, J. Nanomater. **2007**, 16.
[38] L. Lutsev, S. Yakovlev, and C. Brosseau, J. Appl. Phys. **101**, 034320 (2007).
[39] P. Toneguzzo, G. Viau, O. Acher, F. Fievet-Vincent, and F. Fievet, Adv. Mater. (Weinheim, Ger.) **10**, 1032 (1998); See also P. Toneguzzo, O. Acher, G. Viau, F. Fievet-Vincent, and F. Fievet, J. Appl. Phys. **81**, 5546 (1997).
[40] V. Bregar, IEEE Trans. Magn. **40**, 1679 (2004).
[41] S. S. Kalarickal, D. Ménard, J. Das, C. E. Patton, X. Zhang, L. C. Sengupta, and S. Sengupta, J. Appl. Phys. **100**, 084905 (2006).
[42] S. Indris, P. Heitjans, H. E. Roman, and A. Bunde, Phys. Rev. Lett. **84**, 2889 (2000).
[43] E. Schlömann, J. Phys. Chem. Solids **6**, 242 (1958).
[44] M. Sparks, *Ferromagnetic Relaxation Theory* (McGraw-Hill, New York, 1964).
[45] S. Mørup and E. Tronc, Phys. Rev. Lett. **72**, 3278 (1994).
[46] C. Deng, Y. Zhang, J. Ma, Y. Lin, and C.-W. Nan, J. Appl. Phys. **102**, 074114 (2007).
[47] M. Pellarin, B. Baguenard, J. L. Vialle, J. Lerme, M. Broyer, J. Miller, and A. Perez, Chem. Phys. Lett. **217**, 349 (1994).
[48] I. Žutić, J. Fabian, and S. D. Sarma, Rev. Mod. Phys. **76**, 323 (2004).